10-15-2002

Further Investigations of a Mesospheric Inversion Layer Observed in the ALOHA-93 Campaign

Tai-Yin Huang
Clemson University

Michael P. Hickey Ph.D.
Embry-Riddle Aeronautical University, hicke0b5@erau.edu

Tai-Fu Tuan
University of Cincinnati

Scholarly Commons Citation

Huang, T.-Y., M. P. Hickey, T.-F. Tuan, E. M. Dewan, and R. H. Picard, Further investigations of a mesospheric inversion layer observed in the ALOHA-93 Campaign, J. Geophys. Res., 107(D19), 4408, doi: https://doi.org/10.1029/2001JD001186

JOURNAL OF GEOPHYSICAL RESEARCH, VOL. 107, NO. D19, 4408, doi:10.1029/2001JD001186, 2002

Further investigations of a mesospheric inversion layer observed in the ALOHA-93 Campaign

Tai-Yin Huang and Michael P. Hickey
Department of Physics and Astronomy, Clemson University, Clemson, South Carolina, USA

Tai-Fu Tuan
Department of Physics, University of Cincinnati, Cincinnati, Ohio, USA

E. M. Dewan and R. H. Picard
Air Force Research Laboratories, Space Vehicles Directorate, Hanscom Air Force Base, Massachusetts, USA

Received 7 August 2001; revised 31 October 2001; accepted 6 November 2001; published 15 October 2002.

[1] Temperature and wind data obtained from a Na wind/temperature lidar operated by the University of Illinois group during the Airborne Lidar and Observations of the Hawaiian Airglow (ALOHA-93) Campaign, previously analyzed by *Huang et al.* [1998] using an isothermal Brunt-Väisälä frequency, have been reexamined to include temperature gradients in the calculation of the Richardson number. In the previous analysis using the isothermal Brunt-Väisälä frequency the existence of convective instability could not be assessed. New analysis shows that the nonisothermal Richardson number preserves some features found previously, with some striking differences noticable at times between 0900 and 1030 UT. The nonisothermal Richardson number becomes negative as early as 0930 UT, indicating conditions conducive to the development of convective instability and turbulence. The possibility that turbulence could exist at times earlier than previously thought explains more satisfactorily the large temperature increase observed before 1000 UT. *INDEX TERMS:* 3332 Meteorology and Atmospheric Dynamics: Mesospheric dynamics; 3384 Meteorology and Atmospheric Dynamics: Waves and tides; 0342 Atmospheric Composition and Structure: Middle atmosphere—energy deposition; 3367 Meteorology and Atmospheric Dynamics: Theoretical modeling; *KEYWORDS:* gravity wave, temperature inversion layer, critical layer, ALOHA-93 Campaign, instability

Citation: Huang T.-Y., M. P. Hickey, T.-F. Tuan, E. M. Dewan, and R. H. Picard, Further investigations of a mesospheric inversion layer observed in the ALOHA-93 Campaign, *J. Geophys. Res.,*, *107*(D19), 4408, doi:10.1029/2001JD001186, 2002.

1. Introduction

[2] Temperature inversion layers in the mesosphere (also known as mesospheric inversion layers (MILs)) have received considerable attention lately, and an excellent review of the phenomenon is given by *Meriwether and Gardner* [2000] and J. W. Meriwether (The mesosphere inversion layer: New results, submitted to *Journal of Atmospheres and Solar-Terrestrial Physics*, 2001). Initially, they were thought to be anomalous atmospheric phenomena. However, recent observations of mesospheric temperature profiles with improved experimental techniques seem to indicate that, contrary to previous belief, they are actually a very common occurrence in the mesosphere/lower thermosphere (MLT) region. The Airborne Lidar and Observations of the Hawaiian Airglow (ALOHA-93) Campaign was a successful coordination of simultaneous measurements of winds, temperature, and airglow in the MLT region [*Gardner*, 1995; *Dao et al.*, 1995; *Taylor et al.*, 1995; *Hecht et al.*, 1995; *Swenson et al.*, 1995; *Tao and Gardner*, 1995]. It provided an excellent opportunity for piecing together diverse data to better understand the MLT region environment.

[3] Using mean wind and temperature data obtained from the Na wind/temperature (W/T) lidar during ALOHA-93 [*Tao and Gardner*, 1995] and the wave measurements of *Swenson et al.* [1995], *Huang et al.* [1998, hereinafter referred to as H98] first proposed and demonstrated that the observed large wind shears were related to the observed MIL. By projecting the wind along the direction of wave propagation they found that the wave with a 35 m/s phase velocity in the NNW direction (obtained from *Swenson et al.* [1995]) would encounter a critical level near 87 km. The Richardson number (*Ri*) was then calculated to infer the stability of the background atmosphere. Figures 1a and 1b in H98 indicate the existence of a correlation between the large wind shear, the region of instability, the locations of peak temperature associated with the MIL, and the gravity wave critical level. On the basis of their analysis they proposed that the MIL could be formed by the following mechanism: A gravity wave deposits wave energy and

0148-0227/02/2001JD001186

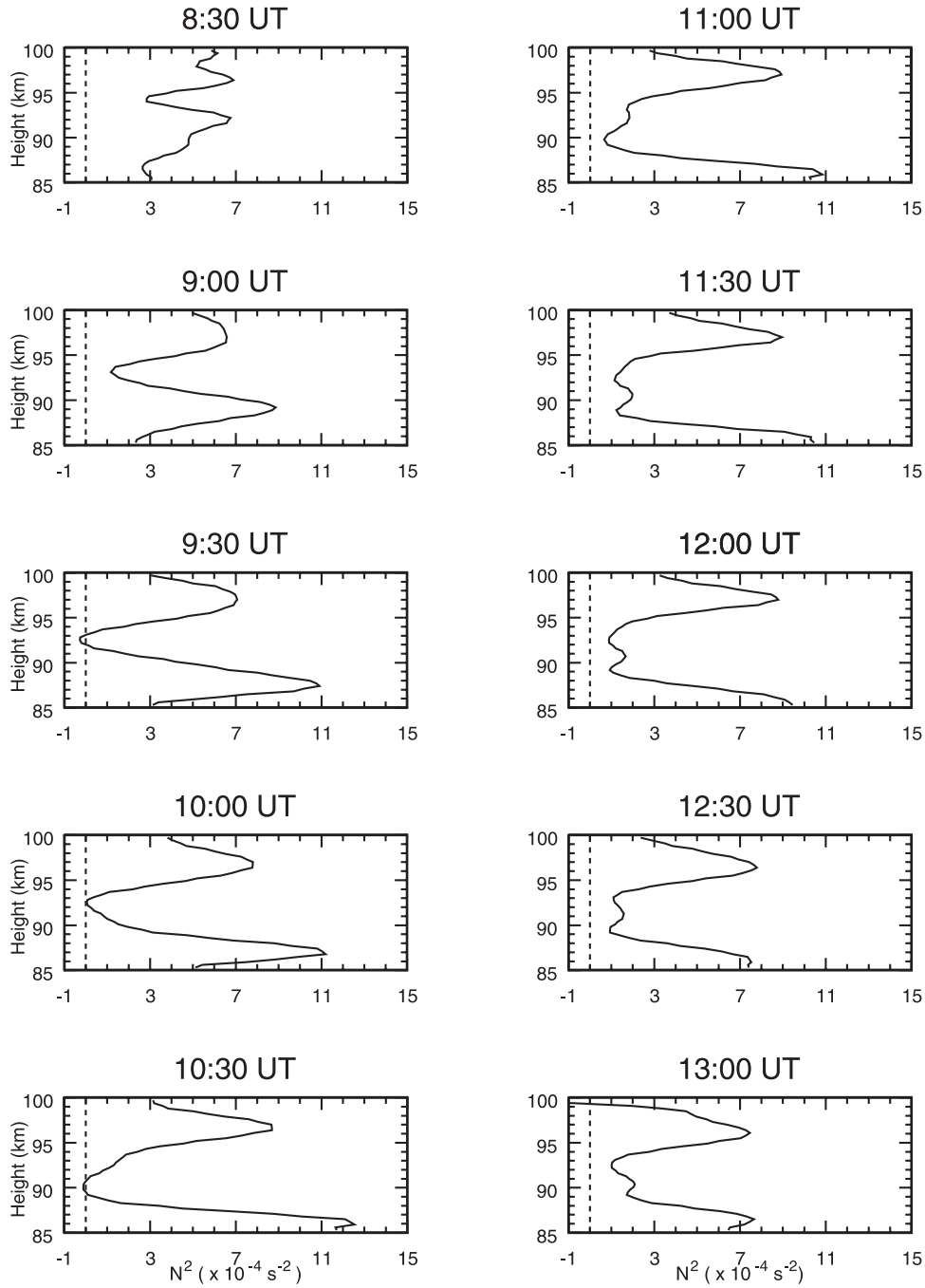

Figure 1. The vertical profile of Brunt-Väisälä frequency squared, N^2, from 0830 to 1030 UT are plotted in the first column and 1100 to 1300 UT in the second column. The dashed vertical line indicates where N^2 becomes zero.

momentum to the mean flow at a critical level. For a strong enough critical level interaction the wind shear increases such that $Ri <\sim 1/4$, a requisite for the onset of dynamical Kelvin Helmholtz (KH), or shear, instability. The amount of heat generated from the dissipation of kinetic energy associated with the mean wind over the region of dynamic instability produces the MIL. Using this hypothesis, H98 estimated that dissipation of mean-state kinetic energy was large enough to account for the temperature increase that was observed by the W/T Na lidar. However, a problem with this hypothesis was that it could not explain the strong temperature increase that was observed to occur before the mean state became unstable (that is, before 1000 UT). Although H98 attributed the temperature increase before 1000 UT to the dissipation of the breaking gravity wave near its critical level, the peak temperature increase occurred several kilometers above the critical level.

[4] It has recently been brought to our attention that the value of *Ri* at 1030 UT in H98 should be less than what was shown in their Figure 1 because the temperature lapse rate appeared to be superadiabatic (J. H. Hecht, private communication, 2000). Consequently, we decided to recal-

culate *Ri* using the nonisothermal Brunt-Väisälä frequency. Additionally, the wind gradient used in the calculation of *Ri* by H98 was that occurring in the presumed direction of wave propagation and was not the total wind gradient required to correctly evaluate the degree of atmospheric stability. The purpose of this paper is to recalculate *Ri* using the nonisothermal Brunt-Väisälä frequency and the total wind gradient, and to reassess the plausibility of the mechanism discussed above in the formation of the observed MIL.

2. Data and Analysis

[5] The Richardson number is calculated using the following equation:

$$Ri = \frac{N^2}{S^2}, \tag{1}$$

where

$$N^2 = \frac{g}{T}\left(\frac{\partial T}{\partial z} + \frac{g}{c_p}\right), \tag{2}$$

$$S^2 = \left|\frac{\partial V_z}{\partial z}\right|^2 + \left|\frac{\partial V_m}{\partial z}\right|^2. \tag{3}$$

Here, N is the Brunt-Väisälä frequency, g is the gravitational acceleration (9.5 m/s^2 in the MLT region) and c_p is the specific heat capacity at constant pressure (1008 J/kg-K) (H98). Also, T is the mean temperature, V_m and V_z are the mean meridional and zonal winds, respectively (as provided by the measurements), and S is the vector wind gradient. The current analysis differs in several ways from that of H98. The main difference is our present use of an altitude-dependent nonisothermal Brunt-Väisälä frequency, that is, the $\partial T/\partial z$ term in equation (2) was not included in H98. In addition, we made several other minor changes such as using an appropriate MLT value for g and the total wind gradient for S (replacing the gradient along a specified direction as in H98). It turns out that most of our calculated values of *Ri* are not strongly dependent on whether we use the definition of S in equation (3) or the definition provided in H98. This is mainly because in our case wind gradients tend to be maximum in the direction of wave propagation, which for this (dominant) wave event corresponded to the NNW direction, most probably as a consequence of wave-mean flow interaction. The largest gradients occurred in a direction near that of the dominant gravity wave propagation direction and persisted for several hours.

3. Results

[6] It is our belief that the wave that was observed by *Swenson et al.* [1995] in the OH airglow (from the aircraft) was not observed over Haleakala because it encountered a critical level there. We further believe that it was the wave-mean flow interaction at this critical level that was responsible for the formation of the MIL observed at Haleakala. The following (revised) results describe the observations, and our interpretation of these observations is provided in the section 4.

[7] The square of the Brunt-Väisälä frequency (N^2) is shown for different times in Figure 1. The profile changes over time, with the initially small trough at 94-km altitude at 0830 UT becoming of much broader vertical extent and deeper at later times. Over the height range of 92–93 km, N^2 becomes negative at times as early as 0930 UT. In this height range it remains negative for ~1 hour, and then at ~1030 UT the region where $N^2 < 0$ moves down to ~90-km altitude. At later times the shape of the N^2 profile resembles a "W" rotated 90 degrees clockwise, having two regions of reduced static stability. It is interesting to note that at 1300 UT at the much higher altitudes of 99–100 km, N^2 becomes negative again. However, because this occurs near the highest altitude of available lidar wind and temperature data where measurement errors are largest, one has to be cautious about its validity. Also, because wind and temperature data were not measured after 1300 UT, we cannot determine if there was another event occurring at higher altitudes.

[8] Figures 2a and 2b are presented in the same fashion as Figures 1a and 1b of H98. The first (wind along the wave direction) and third columns (the temperature profile) are the same as those shown in Figures 1a and 1b of H98. Improved values of *Ri* are plotted in the middle column, as discussed in the previous section. The short dashed horizontal line denotes the location of the critical layer. The long dashed vertical line indicates where the mean flow becomes unstable, i.e., where $Ri < 1/4$. The most striking difference between these results and those of H98 is that the new value of *Ri* is less than zero at several times, indicating the existence of conditions favorable for convective instability. This is a direct result of N^2 being negative, as seen in Figure 1. This was not recognized in H98. The first appearance of negative *Ri* is at 0930 UT at 92–93 km altitude, and at that time the region of dynamical (shear) instability (where $Ri < 1/4$) extends from 91- to 93-km altitude. A half-hour later, at 1000 UT, *Ri* becomes positive everywhere and the region of dynamical instability broadens and extends from 88- to 93-km altitude. This is accompanied by an explosive growth of the wind shear in the direction of the wave vector. The region between 91- and 92-km altitude remains unstable, because once initiated, instability persists as long as $Ri < 1$ [*Businger*, 1969]. At 1030 UT, *Ri* becomes negative again from 89- to 91-km altitude and is less than $1/4$ over the height range 87 to 91 km. For times up until ~1130 UT *Ri* remains $\leq 1/4$ over the height range of 87–88 km. At later times and for altitudes less than ~99 km the atmosphere becomes progressively more stable, although regions with $Ri < 1$ persist over limited height ranges for the duration of the available data. Above 99-km altitude at 1300 UT, *Ri* becomes strongly negative as a consequence of N^2 becoming negative (as discussed earlier).

[9] The wave-mean flow interaction increases the mean shear in the direction of horizontal phase propagation, altering the shape of the mean wind altitude profile. The stronger and longer duration this interaction is the larger the shear may become. Therefore the altitude profile of the shear helps determine the wave propagation direction and the location where the waves would most likely interact with the mean flow. Figure 3 shows a series of contour plots (for times ranging from 0830 to 1300 UT) of the absolute value of shear over 0.3-km intervals as a function of altitude and azimuth. In these figures, azimuth (in degrees) is

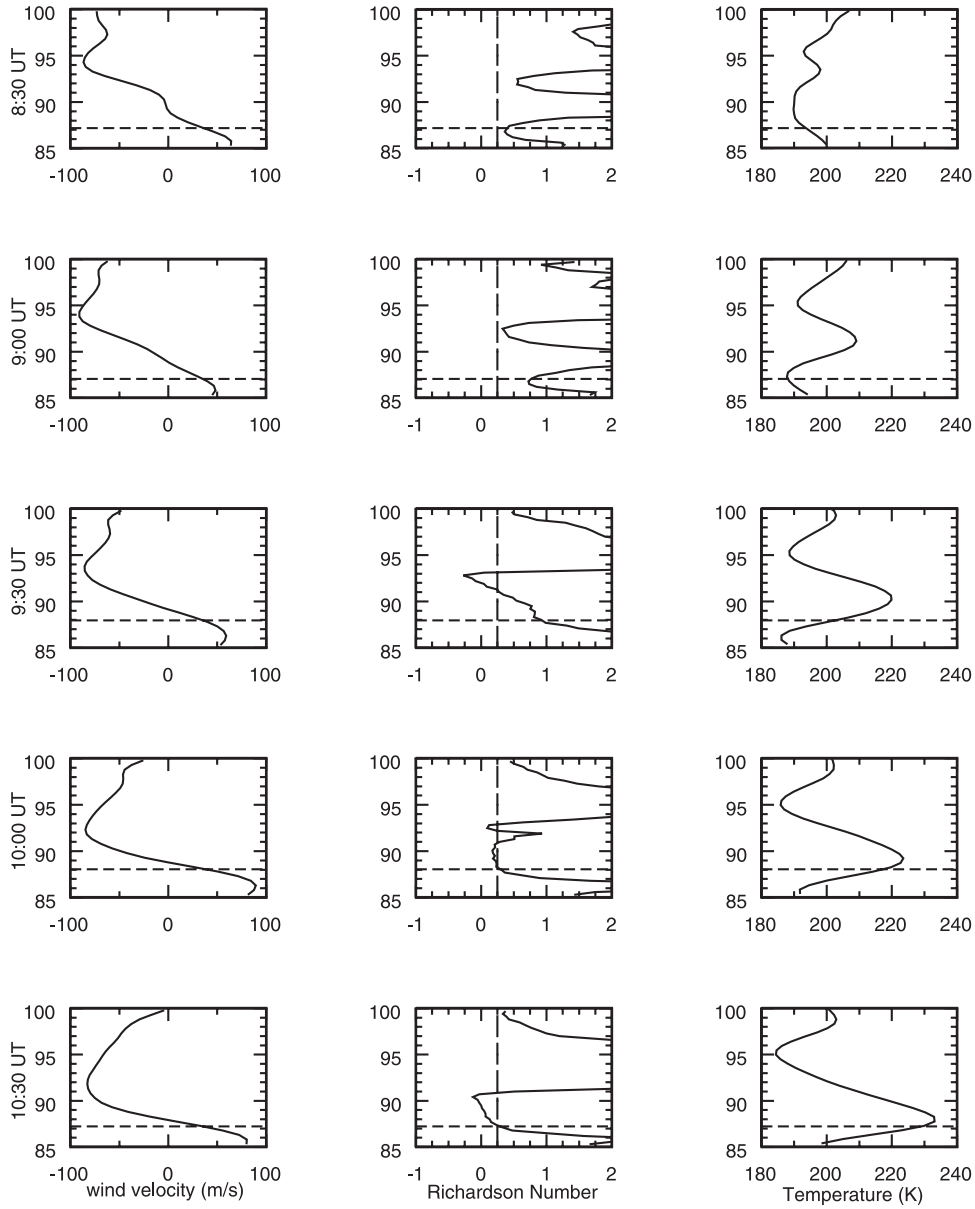

Figure 2a. Wind projected in the wave direction, the Richardson number, and the temperature are plotted in the left, middle, and the right columns, respectively, from 0830 to 1030 UT. The horizontal dashed line indicates the location of the critical level, and the vertical long dashed line denotes the onset of the instability of the mean flow. Ordinate is the altitude in km.

measured in a clockwise direction with north being 0°. For presentation purposes the actual values of the shear in s^{-1} have been multiplied by a factor of 10^3. For a given direction the shear was calculated by first projecting the wind in that direction, then taking the vertical gradient.

[10] The results presented in Figure 3 show that the shear has a very distinctive distribution in height and in azimuth. Between 0830 and 1200 UT and for altitudes above 95 km the shear maximizes at azimuths of ~90° and 270°. At the same times and for altitudes below 95 km the shear maximizes at azimuths of ~160° and 340°. The shear occurring at an azimuth of 90° (160°) is identical to the shear occurring at 270° (340°), since the shear depends only on the magnitude of the horizontal wave vector $\vec{k}$ and hence has period 180°. The shear occurring above 95-km altitude appears to be ~90° out of phase with the shear occurring below 95-km altitude. Note also that the shear (with a lesser strength) near 85-km altitude is ~90° out of phase with the shear occurring above 86-km altitude from 1000 to 1130 UT. In the airglow region (87 to 88 km) maximum shears occur for times between 1000 and 1130 UT. During this period the strength of the shear increases with time and also moves slowly downward toward the peak of the OH airglow region until 1100 UT, after which the shear weakens while remaining at approximately the same altitude. Vertical motion on this night was quite complicated and cannot be simply explained by just accounting for the vertical tidal motions or the vertical fluid velocity, as was discussed in great detail in H98. A local minimum in wind shear is seen to occur in the region between ~91- and

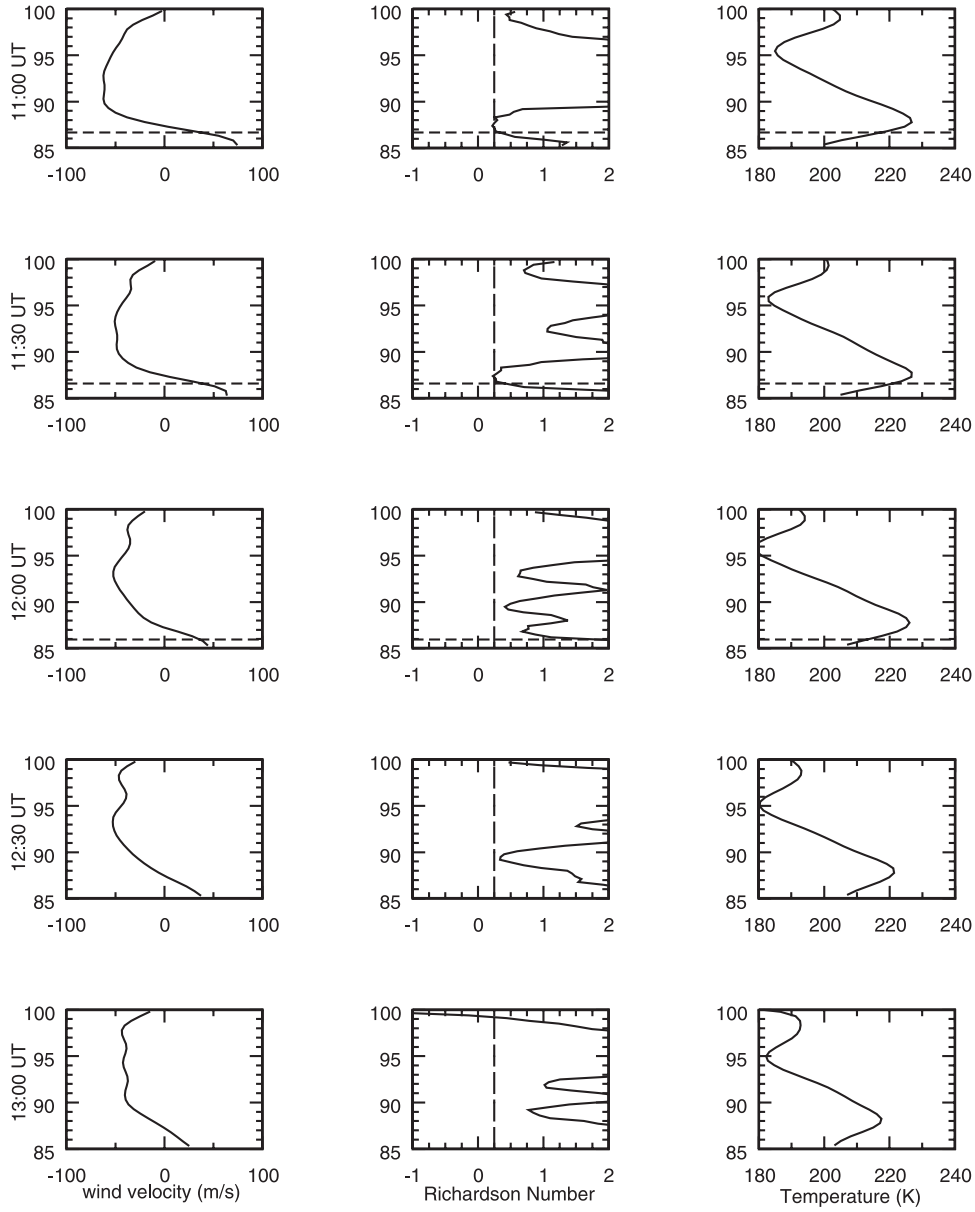

Figure 2b. Same as Figure 2b from 1100 to 1300 UT.

95-km altitude for all azimuths after 1000 UT. At later times this region broadens, with the lower boundary of minimum shear moving down to ~89-km altitude and the upper boundary of minimum shear moving upward to ~96-km altitude. This occurs as a consequence of a broadening at late times in the region of local minimum velocity (see, for example, the wind profile shown in Figure 2b at 1300 UT). Additionally, a close examination of both Figures 1 and 3 shows small (large) values of shear are associated with the occurrence of small (large) values of N^2 at a given altitude. The correlation is most prominent after 1000 UT. Although intuitively we expect more instability would be associated with a small value of N and vice versa, it has been pointed out by *VanZandt and Fritts* [1989] that the opposite is the case. Actually, when a gravity wave propagates from a region of higher static stability to a region of lower static stability, the wave is refracted, the vertical wavelength increases, and the dynamic stability of the atmosphere increases. Therefore the correlation of lower Ri and higher N is not surprising.

[11] Several interesting features previously discussed to some extent by H98 can also be seen in the temperature profiles of Figures 2a and 2b. First, the temperature-inversion layer develops rapidly for the first half of the night (0830–1030 UT), with the peak temperature rising by ~10 K every half-hour except from 0930 to 1000 UT, when a more modest increase occurs. Simultaneously, the altitude of peak temperature moves down ~1 km every half hour except from 0830 to 0900 UT, when a 2-km descent occurs. Second, the peak temperature for the second half of the night (1100–1300 UT) generally undergoes a steady decline. The location of the peak appears to remain essentially fixed at 87-km altitude with only a slight variation in time. Third, the projection of the wind in the direction of

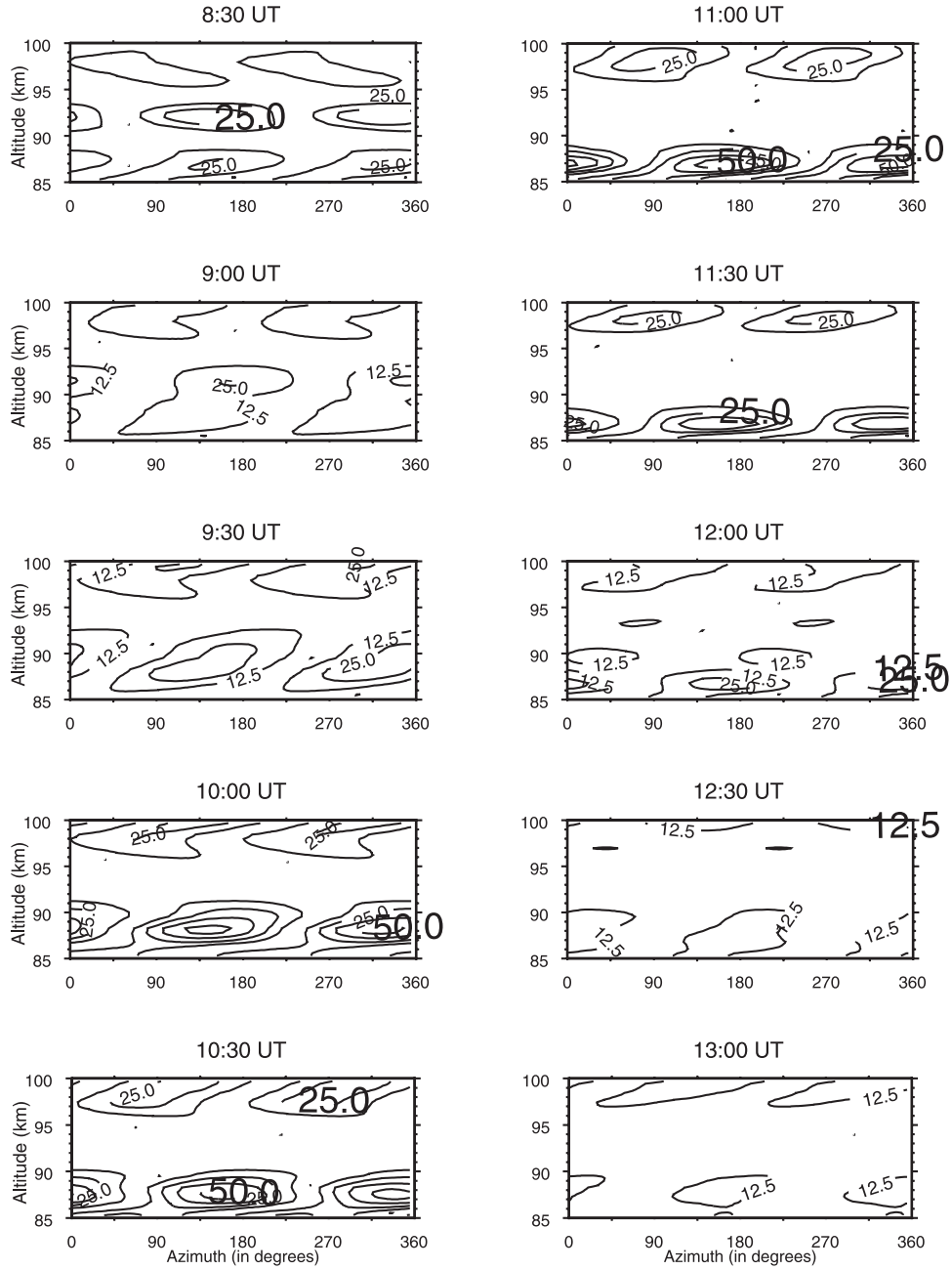

Figure 3. Contour plots of the absolute value of shear (m s^{-1} m^{-1}). The horizontal axis is azimuthal angle, spanning from 0 to 360°, and the vertical axis is the altitude. Winds were projected in particular direction, then shear was calculated in that direction. The patterns repeat every 180° because only the magnitude of the directional shear is plotted.

wave propagation (NNW) shows that the wave would encounter a critical level near the OH airglow region, while below the critical level the wind is much greater than the 35 m/s gravity-wave phase velocity. The wind magnitude at lower altitudes (~85–86 km) exceeds 50 m/s until after 1200 UT. The implication is that a wave propagating upward from below with a 35 m/s phase velocity would be blocked from entering the airglow region. Fourth, the region of strongest convective instability, as identified on the basis of calculated values of *Ri*, is always situated above the critical level throughout the night. The temperature peak occurs slightly below the most unstable region and always occurs above the critical level. Fifth, the strongest shear always lies slightly above the critical level.

4. Discussion

[12] The fact that the temperature data has an uncertainty that depends on altitude and which varies from 1.9 to 0.75 K [*Tao and Gardner*, 1995] introduces uncertainty into our calculated values of *Ri*. Therefore, when discussing the existence of convective and shear instabilities and their relation to values of *Ri* that are very close to either zero, 1/4 or unity, it is possible that in some instances the

atmosphere could be inferred to be unstable when in fact it is slightly stable. A particular example of this can be seen in Figure 2a at 1000 UT, where *Ri* is small and positive near 93-km altitude. We cannot say with complete certainty that the atmosphere was convectively stable at this time and altitude.

[13] The gravity wave of interest to us ($T \sim 38$ min, $\lambda_x \sim 75$ km, direction of propagation $\sim 20^\circ$ west of north) was observed by *Swenson et al.* [1995] in the OH airglow from 1033 UT (on 21 October 1993) when the aircraft was $\sim 7^\circ$ north of Haleakala until 1433 UT when the aircraft was $\sim 2^\circ$ west of Haleakala. Airglow observations from Haleakala showed no signs of this particular wave (M. J. Taylor, private communication, 2001; J. H. Hecht, private communication, 2001), although signs of instability were noticed in the OH airglow (J. H. Hecht, private communication, 2001). To explain these observations, we propose the plausible hypothesis that the gravity wave observed by *Swenson et al.* [1995] encountered a critical level over Haleakala and that the interaction of this wave with the mean flow was the cause of the observed MIL over Haleakala. This hypothesis is based on our belief that the wind variation with location was significant (contrary to the assumption of *Swenson et al.* [1995]) to the extent that a critical level either did not exist at the locations and times of the observations of *Swenson et al.* [1995] or occurred at a significantly different altitude than over Haleakala. To offer some support to this hypothesis, we note that *Dao et al.* [1995] and *Tao and Gardner* [1995] reported strong wind shears at Haleakala. A polar plot of these winds occurring at 1030 UT presented by HT98 reveals a strong reversal of the meridional wind component: Between 87- and 90-km altitude it varies from ~ 50 m/s northward to ~ 50 m/s southward. Therefore, although the height of the critical level was ~ 87.3 km as inferred from the Haleakala winds, we have no wind information at other locations to allow us to infer the existence of critical levels there. Nevertheless, tidal variability and other influences associated with changes in latitude and time should easily suffice to change the altitude location of the critical level of this wave.

[14] We also note that the calculated critical layer over Haleakala occurs directly in the middle of the OH Meinel emission layer. Given the reasonable hypothesis that a critical level did exist for this wave at Haleakala, then we would not expect to readily observe this wave in the OH airglow above Haleakala. This is because its vertical wavelength would be significantly shortened in the vicinity of the critical level, a phenomenon discussed for example by *Gossard and Hooke* [1975, p. 178]. Because the airglow brightness observed at the ground represents a height-integral of the airglow volume emission rate (VER), strong cancellation between airglow VER fluctuations occurring at different altitudes will occur for waves of short vertical wavelength, which will considerably reduce the observable brightness fluctuations. We have verified this claim using the full-wave model of *Hickey et al.* [1997, 1998]. Calculations (not shown) obtained using this model to determine the OH Meinel airglow response to the gravity wave seen in the airborne images of *Swenson et al.* [1995] explored the presence of the critical level in the OH layer. Indeed, we find that the OH column-integrated VER (brightness) fluctuation is reduced by a factor of ~ 50 due to the presence of the critical layer at 87.3 km. This confirms the hypothesis that the wave should be essentially unobservable in the Haleakala images due to destructive interference, or cancellation, of the wave-induced emission fluctuations. This interference results from the shortening without limit of the vertical wavelength as the critical level is approached. We reiterate that it is our belief that the reason *Swenson et al.* [1995] observed the wave at all is because there was no critical level near 87.3-km altitude (nor perhaps in the OH layer at all) above the aircraft flight path during the wave observations. However, there are no observations of winds other than those at Haleakala that allow us to confirm this.

[15] The period of the wave and the integration time for the data (38 min and 15–45 min, respectively) are such that the wave will be only partially averaged out in the lidar wind and temperature profiles. The result is that the lidar profiles will not be exactly ''background'' or ''mean'' profiles but will have some ''contamination'' from the wave, as was discussed in H98.

[16] Temporal variations associated with the tides must be present in the data, since the gravity wave interacts with a mean flow that includes the tides. H98 appealed to the pseudotide phenomenon of *Walterscheid* [1981] to point out that the gravity-wave critical-layer interaction mechanism will be strongly affected by the presence of tides (see also *Liu and Hagan* [1998], *Liu et al.* [1999, 2000], and *Meriwether and Gardner* [2000]). Although the downward progression of features seen in the figures [*Dao et al*, 1995] may appear to be of tidal origin at early times (before 1000 UT), tides cannot explain the observed essentially unchanging nature of these same features at later times. To explain the latter, one must also consider the vertical fluid velocity measured by the Na lidar [*Tao and Gardner*, 1995], not all of which is of tidal origin. We note again (H98) that the actual motion of a feature is quite complex, since there are vertical fluid motions occurring on gravity-wave, tidal, and longer scales and phase motions on gravity-wave and tidal scales.

[17] It is interesting that the temperature profile observed at 0830 UT does not resemble the temperature profile observed at subsequent times. At 0830 UT the local maximum temperature of ~ 198 K occurs at an altitude of ~ 93.5 km, while at 0900 UT the local maximum temperature is ~ 12 K greater and occurs at an altitude ~ 2 km lower near 91.5 km. Furthermore, at 0830 UT it occurs ~ 6 km above the critical layer for the gravity wave parameters considered here, while the *Ri* profile indicates no sign of dynamical or convective instability. The apparent downward velocity of this feature (~ 1 m/s) is too fast to be explained by the diurnal tide (~ 0 at 20° latitude and <30 cm/s at the equator). Although this speed can be explained by the semidiurnal tide, its amplitude should not be this large at these altitudes. A suitable explanation for these rapid changes observed between 0830 and 0900 UT cannot be given because we have no information before the measurements began at ~ 0830 UT.

[18] As previously discussed, an explanation for the origin of MILs based solely on tides is difficult to accept because typical tidal temperature amplitudes are several times smaller than the observed MIL temperature amplitudes. However, tides may play a significant role in MIL development when gravity waves are also considered. Both

of these points were discussed in H98. Recent numerical studies by *Liu and Hagan* [1998], *Liu et al.* [1999], *Liu* [2000], and *Liu et al.* [2000] have shown that the interactions of gravity waves with tides can produce features that closely resemble MIL's. In the simulations of Liu and colleagues, the wave breaking process, which is modulated by the tides, generates large heat fluxes. Generally, these simulations seem to support the claim of H98 that MILs are associated with critical layer interactions between gravity waves and tidally modulated mean flows. However, it is clear that the detailed mechanisms involved require further study.

[19] We have used the full-wave model to estimate the amount of energy (kinetic energy plus available potential energy) carried by the gravity wave, and then determined the energy density within a vertical column extending from 87- to 95-km altitude. Our results (not shown) suggest that the wave carries enough energy to account for the change in the mean state kinetic energy over the same height range. These results are consistent with the observed wind accelerations. Further support can be found in recent numerical simulations of this event which suggest that gravity wave-mean flow interaction could indeed explain the salient features of the observations [*Hur et al.*, 2002]. See also *Dewan and Picard* [2001] for the estimation of wind acceleration in connection with bore theory.

5. Summary and Conclusions

[20] The omission of temperature gradients in the calculation of N^2 by H98 caused their calculated values of *Ri* to be necessarily positive at all times and altitudes. Additionally, their results showed that the mean flow became dynamically unstable only after 1000 UT. We have recalculated *Ri* with nonisothermal N^2 and found that its vertical variation is, to some extent, similar to that found in H98. However, by including temperature gradients in our calculations we have shown that the mean flow becomes convectively unstable as early as 0930 UT, a time for which the atmosphere was originally thought to be stable. On the basis of their analysis, H98 proposed a model to explain the sudden temperature rise as a result of gravity-wave critical-layer interaction. They estimated the heat energy associated with the KH instability and found that it was sufficient to produce the observed temperature increase. However, the large temperature increase observed before the mean flow was thought to become unstable (that is, before 1000 UT) could not be satisfactorily explained at that time. Our newly calculated values of *Ri* based on the nonisothermal Brunt-Väisälä frequency allow us to understand the phenomenon better, while providing stronger support for the original suggestion of H98. At 0930 UT we now find that *Ri* is not only less than 1/4, but that it becomes negative at some altitudes, where N^2 becomes <0. This means that over limited height ranges the atmosphere is more unstable than previously thought. Because motions associated with convective instability should be more energetic than those associated with shear instability, there should be even somewhat more heat energy available to cause the observed increase in temperature than estimated by H98.

[21] **Acknowledgments.** We would like to thank Jim Hecht for bringing this matter to our attention, and for his constructive comments. T.Y.H. was supported by NSF CEDAR grant ATM-0003156, and M.P.H. was supported by NSF grant ATM-9816159 and also through the CEDAR Program by NSF grant ATM-0086299. E.M.D. and R.H.P. acknowledge support from Kent Miller of the Air Force Office of Scientific Research.

References

Businger, J. A., On the energy supply of clear air turbulence, in *Clear Air Turbulence and its Detection*, pp. 100–108, Plenum, New York, 1969.

Dao, P. D., R. Farley, X. Tao, and C. S. Gardner, Lidar observations of the temperature profile between 25 and 103 km: Evidence of strong tidal perturbation, *Geophys. Res. Lett.*, *22*, 2825–2828, 1995.

Dewan, E. M., and R. H. Picard, On the origin of atmospheric bores, *J. Geophys. Res.*, *106*, 2921–2927, 2001.

Gardner, C. S., Introduction to ALOHA/ANLC-93: The 1993 Airborne Lidar and Observations of the Hawaiian Airglow/Airborne NoctiLucent Cloud Campaigns, *Geophys. Res. Lett.*, *22*, 2789–2792, 1995.

Gossard, E. E., and W. H. Hooke, *Waves in the Atmosphere*, Elsevier Sci., New York, 1975.

Hecht, J. H., S. K. Ramsay Howat, R. L. Walterscheid, and J. R. Isler, Observations of variations in airglow emissions during ALOHA-93, *Geophys. Res. Lett.*, *22*, 2817–2820, 1995.

Hickey, M. P., R. L. Walterscheid, M. J. Taylor, W. Ward, G. Schubert, Q. Zhou, F. Garcia, M. C. Kelley, and G. G. Shepherd, Numerical simulations of gravity waves imaged over Arecibo during the 10-day January 1993 campaign, *J. Geophys. Res.*, *102*, 11,475–11,490, 1997.

Hickey, M. P., M. J. Taylor, C. S. Gardner, and C. R. Gibbons, Full-wave modeling of small-scale gravity waves using Airborne Lidar and Observations of the Hawaiian Airglow (ALOHA-93) O(1S) images and coincident Na Wind/Temperature Lidar measurements, *J. Geophys. Res.*, *103*, 6439–6453, 1998.

Huang, T. Y., H. Hur, T. F. Tuan, X. Li, E. M. Dewan, and R. H. Picard, Sudden narrow temperature-inversion-layer formation in ALOHA-93 as a critical-layer-interaction phenomenon, *J. Geophys. Res.*, *103*, 6323–6332, 1998.

Hur, H., T. Y. Huang, Z. Zhao, P. Karananayaka, and T. F. Tuan, A theoretical model analysis of the sudden narrow temperature-layer formation observed in the ALOHA-93 Campaign, *Can. J. Phys.*, in press, 2002.

Liu, H.-L., Temperature changes due to gravity wave saturation, *J. Geophys. Res.*, *105*, 12,329–12,336, 2000.

Liu, H.-L., and M. E. Hagan, Local heating/cooling of the mesosphere due to gravity wave and tidal coupling, *Geophys. Res. Lett.*, *25*, 2941–2944, 1998.

Liu, H.-L., P. B. Hays, and R. G. Roble, A numerical study of gravity wave breaking and impacts on turbulence and mean state, *J. Atmos. Sci.*, *56*, 2152–2177, 1999.

Liu, H.-L., M. E. Hagan, and R. G. Roble, Local mean state changes due to gravity wave breaking modulated by the diurnal tide, *J. Geophys. Res.*, *105*, 12,381–12,396, 2000.

Meriwether, J. W., and C. S. Gardner, A review of the mesosphere inversion layer phenomenon, *J. Geophys. Res.*, *105*, 12,405–12,416, 2000.

Swenson, G. R., M. J. Taylor, P. J. Espy, C. Gardner, and X. Tao, ALOHA-93 measurements of intrinsic AGW characteristics using airborne airglow imager and groundbased Na Wind/Temperture lidar, *Geophys. Res. Lett.*, *22*, 2841–2844, 1995.

Tao, X., and C. S. Gardner, Heat flux observations in the mesopause region above Haleakala, *Geophys. Res. Lett.*, *22*, 2829–2832, 1995.

Taylor, M. J., Y. Y. Gu, X. Tao, C. S. Gardner, and M. B. Bishop, An investigation of intrinsic gravity wave signatures using coordinated lidar and nightglow image measurements, *Geophys. Res. Lett.*, *22*, 2853–2856, 1995.

VanZandt, T. E., and D. C. Fritts, A theory of enhanced saturation of the gravity wave spectrum due to increases in atmospheric stability, *Pure Appl. Geophys.*, *130*, 399–418, 1989.

Walterscheid, R. L., Inertio-gravity wave induced accelerations of mean flow having an imposed periodic component: Implications for tidal observations in the meteor region, *J. Geophys. Res.*, *86*, 9698–9706, 1981.

E. M. Dewan and R. H. Picard, Air Force Research Laboratories, Space Vehicles Directorate, Hanscom AFB, MA 01731-3010, USA.

T.-Y. Huang and M. P. Hickey, Department of Physics and Astronomy, Clemson University, Clemson, SC 29634, USA. (thuang@hubcap.clemson.edu)

T.-F. Tuan, Department of Physics, University of Cincinnati, Cincinnati, OH 45221, USA.